Revealing the Molecular Determinants of Neurotoxin Specificity for Calcium-Activated versus Voltage-Dependent Potassium Channels

Kathleen M. Giangiacomo,*,‡ Jennifer Becker,‡ Christopher Garsky,‡ John P. Felix,§ Birgit T. Priest,§ William Schmalhofer,§ Maria L. Garcia,§ and Theodore J. Mullmann‡

Biochemistry Department, Temple University School of Medicine, 3420 North Broad Street, Philadelphia, Pennsylvania 19140, and Department of Ion Channels, Merck Research Laboratories, Rahway, New Jersey 07065

Received January 24, 2007; Revised Manuscript Received March 12, 2007

ABSTRACT: Potassium channel dysfunction underlies diseases such as epilepsy, hypertension, cardiac arrhythmias, and multiple sclerosis. Neurotoxins that selectively inhibit potassium channels, α-KTx, have provided invaluable information for dissecting the contribution of different potassium channels to neurotransmission, vasoconstriction, and lymphocyte proliferation. Thus, α-KTx specificity comprises an important first step in potassium channel-directed drug discovery for these diseases. Despite extensive functional and structural studies of α-KTx−potassium channel complexes, none have predicted the molecular basis of α-KTx specificity. Here we show that by minimizing the differences in binding free energy between selective and nonselective α-KTx we are able to identify all of the determinants of α-KTx specificity for calcium-activated versus voltage-dependent potassium channels. Because these determinants correspond to unique features of the two types of channels, they provide a way to develop more accurate models of α-KTx−potassium channel complexes that can be used to design novel selective α-KTx inhibitors.

Large-conductance, calcium-activated potassium (BK) channels and voltage-gated potassium (KV) channels are important regulators of neuronal excitability, muscle tone, and lymphocyte proliferation (*1*−*5*), and the potassium channel peptide inhibitors from scorpions, α-KTx, that select between these two channels have been critical in revealing their distinct roles in these processes (*2*, *6*−*9*). Iberiotoxin (IbTX)[1] is the universal selective α-KTx inhibitor of BK channels. Its specificity is defined by the large differences in binding free energy for KV versus BK channels, >6.5 kcal/mol (*7*). In contrast, nonselective α-KTx inhibitors, such as charybdotoxin (ChTX), display negligible differences in binding free energy for BK and KV channels (*7*). Because the α-carbon backbone structures of IbTX and ChTX are nearly superimposable (Figure 1a), the differences in specificity must arise from differences in the amino acid side chains located in five discrete domains (I−V) (Figure 1b). By substituting residues from ChTX into IbTX and examining the effects of these IbTX mutants on their interaction with KV1.3 and BK channels, we were able to identify all of the determinants of IbTX specificity.

* To whom correspondence should be addressed. E-mail: giang@temple.edu. Phone: (215) 707-8170. Fax: (215) 707-3263.

‡ Temple University School of Medicine.

§ Merck Research Laboratories.

[1] Abbreviations: α-KTx, peptide toxin potassium channel inhibitor; [^{125}I]-α-KTx, α-KTx labeled with ^{125}I; IbTX, iberiotoxin or α-KTx1.3, charybdotoxin; ChTX or α-KTx1.1 [^{125}I]HgTX, mutant of hongotoxin, A19Y/Y37F, labeled with ^{125}I at Y19; [^{125}I]-IbTX, mutant of IbTX, D19Y/Y36F, labeled with ^{125}I at Y19.

MATERIALS AND METHODS

Recombinant α-KTx Peptides. Plasmids pG9IbTX-S10A, pG9AgTX2-D20C, and pG10ChTX-R19C encoding T7 gene 9, a factor Xa cleavage site, and genes for IbTX-S10A (*10*), AgTX2 (*11*), and ChTX (*12*), respectively, were used to generate mutant toxins as described. pG9AgTX2-D20C, a gift from M. Kohler (Merck Research Laboratories) was mutated to AgTX2-C20D (wild type). pG9ChTX-R19C, provided by C. Miller (Brandeis University, Waltham, MA) was mutated to ChTX-R19Y-Y36F. The identity of all constructs was verified by dideoxy sequencing (Nucleic Acid Facility, Kimmel Cancer Institute, Philadelphia, PA). *Escherichia coli* strain BL21(DE3) harboring these plasmids was cultured and induced, and the recombinant protein was purified by ion exchange and HPLC as described previously (*10*). Cyclization of the N-terminal glutamine in IbTX and ChTX mutants and purification were performed as described previously (*10*). The identity of each peptide was verified by MALDI-MS mass spectrometric analysis (Commonwealth Biotechnologies). IbTX-S10A is termed wild-type IbTX throughout this work and was purified previously (*10*). The predicted and measured molecular weights for each peptide were as follows: 4090.93 and 4090.35 for AgTX2, 4034 and 4034.58 for AgTX2-N30G, 4287 and 4287.9 for ChTX-R19Y/Y36F, 4275 and 4276.2 for ChTX-R19Y/N30G/Y36F, 4289 and 4287 for IbTX-G30N, 4244 and 4242 for IbTX-D24S/G30N, 4260 and 4258.17 for IbTX-D4N/D6S/G30N, 4232 and 4230.38 for IbTX-D4N/D6S/D24S/G30N, 4293 and 4291.47 for IbTX-(FVGD$_{21-24}$HNTS)-G30N, and 4260 and 4260.37 for IbTX-S8T/V9T/D24S/G30N, respectively. ChTX and IbTX used in binding assays were from Peptides International.

10.1021/bi700150t CCC: $37.00
Published on Web 04/18/2007

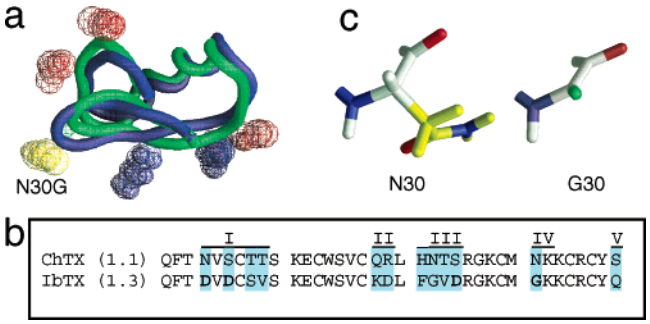

FIGURE 1: Sequence differences between selective (IbTX) and nonselective (ChTX) toxins underlie specificity determinants for BK channels vs KV channels. (a) Overlay of ChTX (blue) and IbTX (green) α-carbon backbones (*30*, *31*). Side chain atoms in IbTX are colored as follows: red for D4, D6, and D24 and blue for K27 and R25. In ChTX, N30 is colored yellow. (b) Amino acid sequences for ChTX and IbTX differ in five discrete regions (shaded). Residues that confer IbTX specificity as shown in this work are in bold. (c) Comparison of side chain atoms in N30 and G30. α-Carbon bonds are colored white, amines blue, and oxygen atoms red. Side chain bonds in N30 are colored yellow; in G30, the single H is colored green. The coordinates for IbTX were provided by B. Johnson (Merck Research Laboratories).

Cell Lines and Transfection. BK channels were transiently transfected into TsA-201 cells (*13*) using the human a clone huR2+ as described previously (*14*). TsA-201 cells were generously provided by V. Ramakrishnan (Protein Design Labs, Inc.). HEK293 cells stably transfected with human clone KV1.3 were maintained as described previously (*15*). CHO cells stably expressing human KV1.3 channels were maintained in T-75 flasks in Iscove's modified Dulbecco's medium supplemented with 10% fetal bovine serum, 1% penicillin-streptomycin, 2 mM L-glutamine, 50 μg/mL G418, and 1% hypoxanthine-thymidine supplement in a humidified 10% CO_2 incubator at 37 °C.

Plasma Membrane Preparation. Membranes from TsA-201 cells expressing the BK channel or HEK293 cells expressing KV1.3 channels were prepared as described previously (*14*, *15*). Sarcolemma membranes from bovine aortic smooth muscle were prepared as described in ref *16*.

Binding Assays. The interaction of mutant toxins with BK and KV1.3 channels was monitored by competitive displacement of [^{125}I]IbTX-D19Y/Y36F ([^{125}I]IbTX) and [^{125}I]-HgTX-A19Y/Y37F ([^{125}I]HgTX), respectively, from membranes expressing these channels, as described previously (*10*). Nonspecific binding was determined in the presence of excess ChTX for KV1.3 channels or excess IbTX for BK channels. Data were computer fitted to a general dose−response equation and analyzed for equilibrium toxin dissociation constant (K_i) values as described previously (*17*). Each determination of K_i was made a minimum of three times, and errors are expressed as the standard error of the mean.

Single-BK Channel Recordings in Planar Lipid Bilayers. Planar lipid bilayers, composed of a 7:3 POPE:POPC molar ratio, were formed, and BK channels from bovine aortic sarcolemmal membranes were fused with the bilayer as described previously (*18*). Solutions bathing both sides of the channel contained 150 mM KCl that eliminates the effects of the β1 subunit on ChTX block of the BK channel (*19*). Currents were detected and amplified using a Dagan 3900A integrating patch clamp amplifier (Dagan Corp.) as described previously (*18*). Single-channel currents were digitally encoded with Pulse (HEKA Electronik, Inc.) onto a Macintosh computer. Single-channel records were refiltered off-line using a digital Gaussian filter in TAC (SKALAR Instruments, Inc.), and events were detected using a threshold algorithm in TAC. Distributions of closed and open times were plotted and fitted using TAC fit (SKALAR Instruments, Inc.), and toxin-blocked times were distinguished from control closed times as described in ref *18*.

Recordings of the Whole-Cell KV1.3 Current. KV1.3 currents were recorded using the IonWorks HT system (Molecular Devices, Sunnyvale, CA) as described previously (*20*). Briefly, hole resistances in the 384-well planar sealchip were approximately 3−4 MΩ. Electrical access to the cytoplasm was achieved by perforation in 0.13 mg/mL amphotericin B for 4 min. The test pulse, consisting of a 400 ms step to 40 mV from a holding potential of −80 mV, was applied before and after a 10 min toxin incubation, during which the cells were not voltage clamped. Data were acquired at 5 kHz. Leak conductances were measured during a 100 ms step from −80 to −70 mV and digitally subtracted. Only cells with membrane resistances of >50 MΩ and peak currents of > 0.5 nA were included in the analysis. The amplitude of the peak current in the presence of toxin, normalized to the peak current in control, was fit to the Hill equation. Toxins were prepared in Dulbecco's phosphate-buffered saline supplemented with 0.05% BSA.

Distance Array Analysis of α-KTx−Channel Complexes. Center-to-center distance arrays were calculated either between the entire toxin and channel molecules or between a subset of atoms for structural models of AgTX2−*Shaker* (*21*) and AgTX2−KV1.3 (*22*) complexes using Grasp (*23*). Coordinates for AgTX2−*Shaker* mode I and AgTX2−*Shaker* mode II were a gift from B. Roux (University of Chicago, Chicago, IL). Coordinates for the ChTX−KV1.3 complex were a gift from H. Jiang (Shanghai Institute for Biomedical Sciences, Shanghai, China).

RESULTS

Unique H-Bond Partners in α-KTx Are Critical for KV Inhibition. All α-KTx that inhibit KV channels with high affinity contain a conserved asparagine, "N30", corresponding to the single amino acid in domain IV (Figure 1) (*10*). In contrast, IbTX contains a glycine at this position, "G30". We previously showed that the IbTX mutant, G30N, exhibited >100-fold tighter binding as an inhibitor of binding of [^{125}I]-α-KTx to membranes expressing KV1.3 channels, decreasing the K_d value from >2000 to 40 nM, suggesting G30 is an important determinant of specificity (*10*). However, K_d values obtained from displacement of [^{125}I]-α-KTx are typically 10−100-fold lower than K_d values obtained from current inhibition, raising the possibility that IbTX-G30N might not potently inhibit KV1 channel current. Using a planar array-based high-throughput patch−clamp technique (*20*), we now show that IbTX-G30N inhibits KV1.3 whole-cell current with a K_d value of 220 nM (Figure 2b,d). In contrast, 3000 nM IbTX has no effect on KV1.3 current (Figure 2a). Thus, the "G30N" mutation decreases the K_d value for KV1.3 channels by >100-fold relative to that of the wild type. The magnitude of these favorable changes in binding free energy for KV1.3 channels (more than −2 kcal/

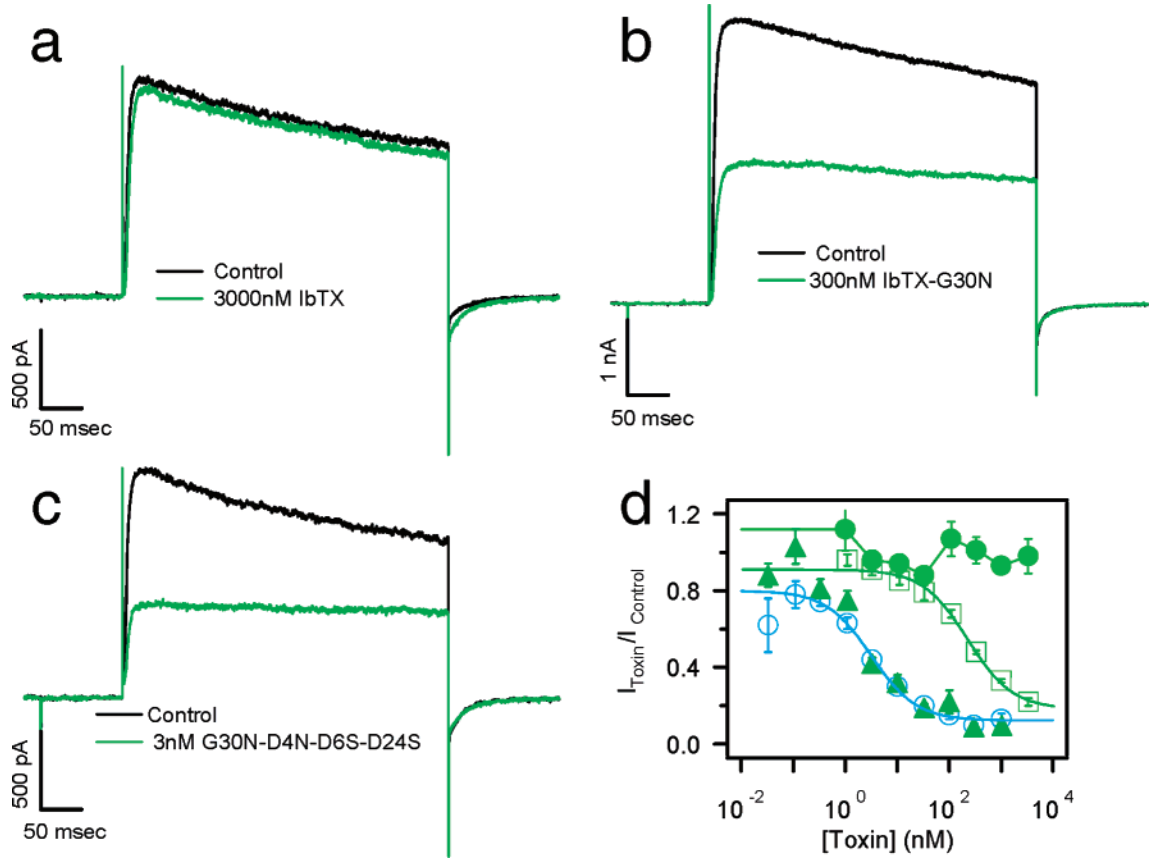

FIGURE 2: Effects of IbTX mutants on the KV1.3 whole-cell current from CHO cells in the absence (control) and presence of (a) 3000 nM IbTX, (b) 300 nM IbTX-G30N, and (c) 3 nM IbTX-G30N/D4N/D6S/D24S. (d) Dose-dependent effects of ChTX (blue empty circles), IbTX (green filled circles), and the IbTX mutants G30N (green empty squares) and G30N/D4N/D6S/D24S (green filled triangles) are plotted as the fraction of current remaining in the presence of toxin relative to control. The line represents the best fit of the data to a generalized binding equation of the form $I_{toxin}/I_{control} = 1 + (K_d/x)^n$, where I_{toxin} and $I_{control}$ are the current amplitudes in the presence and absence of a given toxin concentration (x), respectively, and K_d is the equilibrium dissociation constant for toxin binding. K_d values obtained from the fits were 3 and 220 nM for ChTX and IbTX-G30N, respectively.

Table 1: Effect of N30G α-KTx Mutants from Three Subfamilies on Competitive Displacement of [^{125}I]HgTX from KV1.3 Channels[a]

toxin	K_i (nM)	$K_{i(mt)}/K_{i(wt)}$	$\Delta\Delta G_{(mt-wt)}$ (kcal/mol)
α-KTx 1.x			
ChTX-R19Y/Y36F	0.027 ± 0.007	1	0
ChTX-R19Y/N30G/Y36F	>900	>33333	>6.2
α-KTx 2.x			
NxTX-ΔN1-ΔC39[b]	1.2 ± 0.4	1	0
NxTX-ΔN1-ΔC39-N30G[b]	>2700	>2250	>4.6
α-KTx 3.x			
AgTX	0.013 ± 0.002	1	0
AgTX-N30G	0.69 ± 0.04	53	>2.35

[a] Membranes were incubated with [^{125}I]HgTX (2200 Ci/mmol) in the absence or presence of unlabeled mutant peptide until equilibrium was achieved. The incubation medium consisted of 100 mM NaCl, 5 mM KCl, 0.1% BSA, and 20 mM Tris-HCl (pH 7.4). Nonspecific binding was determined in the presence of 30 nM ChTX (Peptides International). [b] Previously published (*10*).

mol) is most consistent with H-bonding interactions. Indeed, the "N30" side chain contains three possible H-bond partners not present in G30 (Figure 1c). Furthermore, the "N30G" mutation in α-KTx from three different subfamilies (ChTX, NxTX, and AgTX) causes an unfavorable change in binding free energy of >2 kcal/mol for KV1.3 channels (see Table 1 for a list of K_d and free energy values). Taken together, these findings suggest that the high-affinity interaction between α-KTx and KV channels depends on unique H-bonding interactions between N30 in the peptide and specific residues in the KV channel outer pore.

Four ChTX-like Mutations in IbTX Promote High-Affinity Inhibition of the KV1.3 Whole-Cell Current. Our data show that G30 in IbTX is a major determinant of specificity, accounting for >2 kcal/mol of the >6.5 kcal/mol difference in binding free energy between BK and KV channels. To identify other amino acids in IbTX that confer specificity, we substituted residues present in ChTX from domains I−IV into IbTX (Figure 1). Because IbTX does not interact with KV1.3 channels without the G30N mutation, we introduced cassette and point mutants into IbTX-G30N. The criterion for identifying all of the IbTX amino acids conferring specificity is satisfied when the IbTX mutant and ChTX display the same high-affinity interaction for KV1.3 channels. IbTX contains three acidic residues, D4 and D6 (both in domain I) and D24 (domain III), unique to BK selective blockers. In addition, previous studies showed that ChTX residues from domains I and III are part of the toxin interaction surface for KV and BK channels while residues from domain II are not (*7*). Remarkably, the IbTX-G30N mutant with the corresponding ChTX residues at these three positions (D4N, D6S, and D24S) inhibits whole-cell KV1.3 currents with a K_d value of 2 nM, nearly identical to that of ChTX. Indeed, this IbTX mutant displays 100-fold higher potency relative to IbTX-G30N (Figure 2 and Table 2). The

Table 2: Effect of ChTX, IbTX, and Mutants on Whole-Cell KV1.3 Currents

toxin	K_i (nM)	$K_{i(mt)}/K_{i(IbTX-G30N)}$	$\Delta\Delta G_{(mt-IbTX-G30N)}$ (kcal/mol)
ChTX	3.2	0.011	−2.64
IbTX	>30000	>139	>2.92
IbTX-G30N	216	1	0
IbTX-D24S/G30N	12.4	0.06	−1.69
IbTX-D4N/D6S/G30N	9.9	0.05	−1.83
IbTX-S8T/V9T/D24S/G30N	6.8	0.03	−2.05
IbTX-D4N/D6S/D24S/G30N	2.1	0.01	−2.74

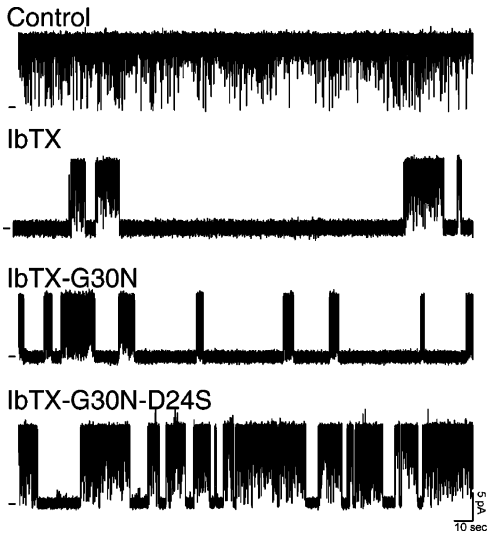

FIGURE 3: Effects of IbTX and mutant peptides on single-BK channel currents in the absence (control) and presence of externally applied toxin. For each trace, closed channel current levels are indicated by the lines to the left, and the channel is open most of the time in the control. Time and current scales are shown. Conditions: 150 mM KCl inside and outside, 300 μM $CaCl_2$ inside, 40 mV.

two IbTX-G30N mutants, D24S and D4N/D6S, each caused an ~10-fold decrease in K_d relative to that of IbTX-G30N, suggesting that the effects of these mutations are independent and additive (Figure 4 and Tables 2 and 3). In addition, the IbTX-G30N cassette mutant with all of the residues from domain II, IbTX-(FVGD$_{21-24}$HNTS)-G30N, caused a similar ~10-fold decrease in K_d relative to that of G30N, suggesting that only D24S in domain II contributes to IbTX specificity (Table 3). In contrast, mutation of two other ChTX-like residues in domain III, T8S/T9V, does not cause a decrease in K_d (Table 2). Similar results were obtained for competitive displacement of [^{125}I]HgTX from membranes expressing KV1.3 channels (Table 3). The structures of these mutant toxins are likely only altered at the site of mutation because the IbTX and ChTX backbone structures are nearly superimposable, suggesting only the side chain structures differ between the two toxins. Also, the independence and additivity of the toxin mutants are consistent with structural changes only at the site of mutation. Taken together, these findings suggest that four residues in IbTX (D4, D6, D24, and G30) underlie its specificity for BK over KV channels.

ChTX-like Mutations in IbTX Have Negligible Effects on the Inhibition of BK Channels. By definition, specificity is defined entirely by the difference in toxin binding free energy for the two different channels. Thus, an amino acid in IbTX confers specificity if mutagenesis minimizes this difference, i.e., if it causes a large favorable change in binding free energy for the KV channel while causing either negligible or unfavorable changes for the BK channel. To test this prediction, we examined the effects of these IbTX mutant peptides on the block of current through single BK channels in planar lipid bilayers. Figure 3 shows that IbTX and the mutants G30N and G30N/D24S cause the appearance of nonconducting silent periods, seconds in duration, interspersed by periods of normal channel activity. The mean duration of these silent or blocked periods is inversely related to the toxin dissociation rate constant (k_{off}), while the mean bursts of channel activity are inversely related to the pseudo-first-order toxin association rate constant (k_{on}[toxin]) (*18*). Mean blocked times for IbTX and the mutants G30N, D24S/G30N, D4N/D6S/G30N, and D4N/D6S/D24S/G30N, averaged from several experiments, are 104, 40, 9, 11, and 6 s, respectively (Table 4). In contrast, the second-order association rate constant (k_{on}) values for these mutants are either similar to or ~3-fold greater than that of the wild type. Thus, the corresponding K_d values for the IbTX mutants G30N, D24S/G30N, D4N/D6S/G30N, and D4N/D6S/D24S/G30N increased by 2-, 14-, 2.7-, and 8-fold, respectively, relative to that of wild-type IbTX (Figure 4b and Table 4). Similar increases in the K_d relative to the wild-type value were obtained from competitive displacement of [^{125}I]IbTX from membranes expressing BK channels (Figure 4 and Table 5). Thus, as predicted, mutation of the IbTX residues underlying specificity, D4, D6, D24, and G30, causes increases in the K_d relative to the wild-type value for the BK channel.

Table 3: Effect of ChTX, IbTX, and Mutants on Competitive Displacement of [^{125}I]HgTX from the KV1.3 Channel[a]

toxin	K_i (nM)	$K_{i(mt)}/K_{i(IbTX-G30N)}$	$\Delta\Delta G_{(mt-IbTX-G30N)}$ (kcal/mol)
ChTX	0.023 ± 0.07	0.0023	−3.6
IbTX	>2700	>270	>3.3
IbTX-G30N	10 ± 2	1	0
IbTX-D24S/G30N	1.2 ± 0.2	0.12	−1.3
IbTX-(FVGD$_{21-24}$HNTS)-G30N	1.2 ± 0.2	0.12	−1.3
IbTX-D4N/D6S/G30N	1.3 ± 0.05	0.13	−1.2
IbTX-S8T/V9T/D24S/G30N	1.6 ± 0.1	0.16	−1.08
IbTX-D4N/D6S/D24S/G30N	0.044 ± 0.004	0.004	−3.2

[a] Assay conditions are as described in footnote a of Table 1.

DISCUSSION

Together, these findings suggest that the differences between IbTX and ChTX at these four positions (D4N, D6S, D24S, and G30N) account for all of the differences in binding free energy and hence IbTX specificity for BK over KV channels. Numerous studies have identified pairwise interactions between α-KTx and KV channel residues (*24*−*27*). However, the corresponding channel partners underlying specificity have not been identified. Our work shows that the identity of the amino acid, "G30N", is a major determinant of specificity, and it supports the notion that "N30" forms critical H-bonds with channel residues that are unique to KV channels. "N30" is strictly conserved among all

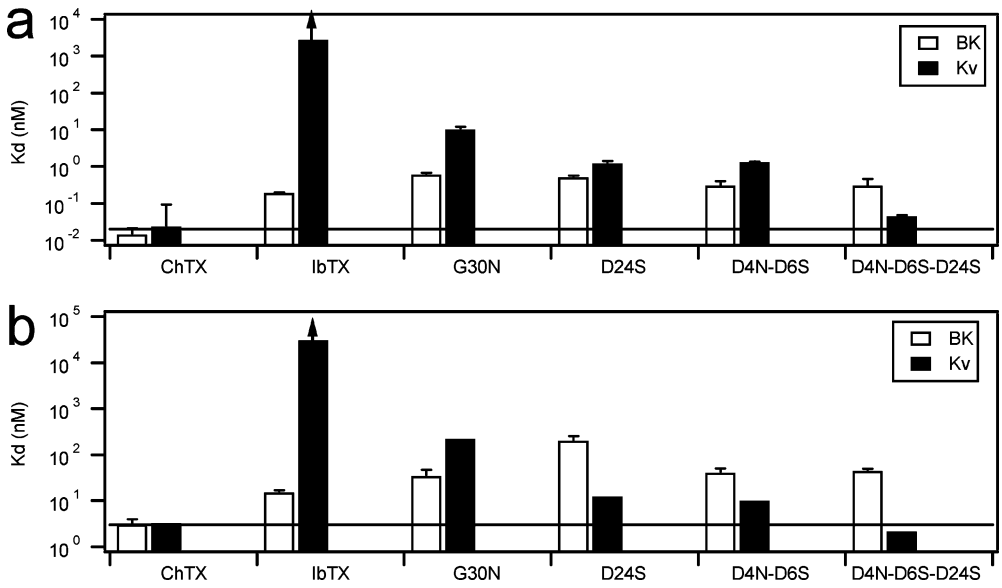

FIGURE 4: Mutation of four residues in IbTX promotes high-affinity KV1.3 binding and weakens BK affinity in [^{125}I]-α-KTx binding displacement (a) and potassium current inhibition (b) assays. (a) K_i values for ChTX, IbTX, and IbTX mutants with BK (white bars) and KV1.3 (black bars) channels were measured by competitive displacement of [^{125}I]IbTX and [^{125}I]HgTX, respectively, from membranes expressing these channels. (b) K_d values for toxin block of BK (white bars) and KV1.3 (black bars) channels were obtained from toxin blocking kinetics of single-BK channel current and from dose-dependent inhibition of whole-cell KV1.3 currents, respectively.

Table 4: Effect of IbTX Mutants on Toxin Blocking Kinetics of Single BK Channels in Planar Lipid Bilayers[a]

toxin	K_d (nM)	$1/k_{off}$ (s)	k_{on} ($\times 10^6$ M^{-1} s^{-1})
UC-IbTX[b]	1400 ± 300	1.5 ± 0.4	0.6 ± 0.3
IbTX	14.6 ± 2	104 ± 40	1.1 ± 0.3
IbTX-G30N	34 ± 13	40 ± 12	1.2 ± 0.2
IbTX-D24S/G30N	200 ± 50	9 ± 3	1.2 ± 0.5
IbTX-D4N/D6S/G30N	40 ± 10	11 ± 5	2.7 ± 0.5
IbTX-S8T/V9T/D24S/G30N	140 ± 50	8 ± 5	1.5 ± 0.6
IbTX-D4N/D6S/D24S/G30N	44 ± 6	8 ± 2	3.3 ± 0.3

[a] The equilibrium dissociation constant, K_d, values were calculated from the first-order dissociation rate constant (k_{off}) and second-order association rate constant (k_{on}) values ($K_d = k_{off}/k_{on}$). Rate constants for toxin block were determined as described in Materials and Methods. Values were averaged from three to six measurements, and errors represent standard errors of the mean. IbTX, used in planar lipid bilayer experiments, refers to a recombinant mutant IbTX, IbTX-S10A, which displays a 10-fold weaker K_d value than the wild type (*10*). [b] UC-IbTX, uncyclized IbTX, has an uncyclized N-terminal glutamine. All other peptides contain a cyclized pyroglutamine at the N-terminus necessary for high-affinity block (*10*).

Table 5: Effect of ChTX, IbTX, and Mutants on Competitive Displacement of [^{125}I]IbTX from the BK Channel[a]

toxin	K_i (nM)	$K_{i(mt)}/K_{i(wt)}$	$\Delta\Delta G_{(mt-wt)}$ (kcal/mol)
ChTX	0.014 ± 0.007	–	–
IbTX	0.19 ± 0.01	1	0
IbTX-G30N	0.6 ± 0.07	3.16	0.68
IbTX-D24S/G30N	0.5 ± 0.07	2.63	0.57
IbTX-D4N/D6S/G30N	0.3 ± 0.1	1.58	0.27
IbTX-S8T/V9T/D24S/G30N	6.6 ± 0.3	34.7	2.1
IbTX-D4N/D6S/D24S/G30N	0.3 ± 0.16	1.58	0.27

[a] Membranes were incubated with [^{125}I]IbTX (2200 Ci/mmol) in the absence or presence of unlabeled mutant peptide until equilibrium was achieved. The incubation medium consisted of 20 mM NaCl, 0.1% BSA, and 20 mM Tris-HCl (pH 7.4). Nonspecific binding was determined in the presence of 100 nM IbTX (Peptides International). IbTX, used in dose-dependent assays, refers to a recombinant mutant IbTX, IbTX-S10A, which displays a 10-fold weaker K_i value than the wild type (*10*).

α-KTx known to inhibit KV channels with high affinity. This remarkable conservation of "N30" suggests that H-bond partners in the channel might be similarly conserved and that the corresponding side chains might serve an important functional role in KV channels. Despite its clear importance in specificity and the large changes in binding free energy caused by its mutation, no functional studies to date have identified the KV channel H-bond partners for "N30" (*24*−*27*). The magnitude of changes in binding free energy caused by either introduction of N30 or its removal (∼2−4 kcal/mol) and the H-bonding capabilities of "N30" are consistent with at least two H-bonds with the channel. These channel H-bond partners could derive from more than one side chain or even backbone atoms. Both possibilities could explain why the corresponding channel interaction partner for "N30" was not identified in previous functional studies.

Correlating α-KTx Specificity Determinants with KV Channel Structure. To identify potential H-bond partners for N30 in KV channels, we applied distance array analysis to structural models of AgTX2−*Shaker* and ChTX−KV1.3 complexes that are based on known, conserved toxin−channel interactions. The structural models of AgTX2 in complex with the *Shaker* KV1 channel (*21*) are based on distance restraints deduced from experimentally determined toxin−channel pairwise interaction energies (*25*). From these computational studies, two different structural models of AgTX2 in complex with *Shaker* (mode I and mode II) were found to be consistent with the experimentally determined interaction energies (*21*). Calculation of center-to-center distances between all "N30" atoms in AgTX2 and all atoms in *Shaker* mode I revealed one possible H-bond between a carboxylate oxygen in E422 (Oϵ2) and an amine hydrogen in N30 (Hδ22) (3.0 Å, Figure 5b). In contrast, for mode II, no H-bonding atoms were within 3.5 Å of atoms in "N30". Conversely, distance array analysis of the ChTX−KV1.3 complex (*22*) revealed two possible H-bonds with a different

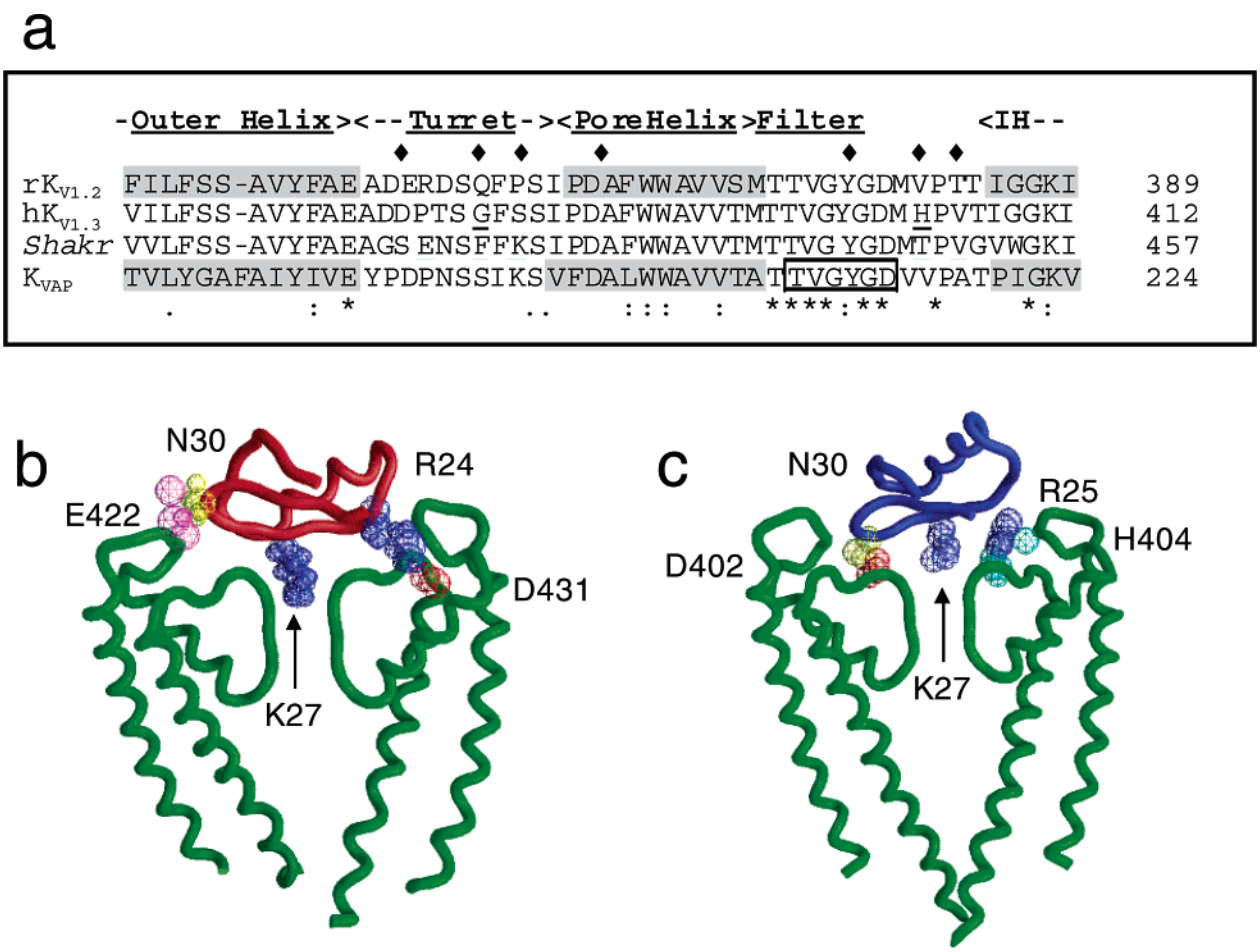

FIGURE 5: Structural models of α-KTx−channel complexes predict two possible H-bond partners for "N30" but no channel partners for amino acids corresponding to D4, D6, or D24 in IbTX. (a) Amino acid sequence alignment of KV1 pore regions and associated secondary structure based on the three-dimensional X-ray crystal structure of rat KV1.2 (*32*) and KVAP (*33*). Asterisks indicate residues strictly conserved across 40 different KV sequences from 24 different species. Diamonds indicate channel residues contributing to the α-KTx binding site (*7*). (b) Structural model of AgTX2−*Shaker* mode I (*21*). Three atoms in *Shaker* E422 (magenta) are within 3.5 Å of N30 (yellow) on AgTX2. No H-bonding partners for "N30" were predicted from distance array analysis AgTX2−*Shaker* mode II. (c) Structural model of the ChTX−KV1.3 complex (*22*). Two H-bond acceptors in KV1.3 D402 (red) are within 3.5 Å of "N30" (yellow) in ChTX. No KV1.3 atoms are within 6 Å of ChTX side chains N4, S6, and S24 that are equivalent to the D4, D6, and D24 side chain positions in IbTX. The highly conserved K27 (blue) in α-KTX interacts with atoms in the selectivity filter.

channel residue, D402 (D447 *Shaker*), located at the extracellular side of the selectivity filter (Figure 5c). Recently, a structural model of the related kaliotoxin (KTX or α-KTx 3.1) in complex with the Kcsa−KV1.3 chimeric channel was deduced from analysis of chemical shifts and proton−proton distances obtained from solid-state NMR (*28*). Unfortunately, in this study, no chemical shift data were recorded for "N30" or consequently for its channel interaction partners. Thus, three models of α-KTx−KV1 channel complexes suggest three different interaction partners with "N30". In addition, only one of these models predicted a H-bond channel partner (D402 of KV1.3 or D447 of *Shaker*) that is strictly conserved among all KV channels. As expected, all models revealed extensive contacts between atoms involved in conserved toxin−channel interactions, such as those of K27 with atoms in the selectivity filter (Figure 5). Taken together, these findings suggest that current structural models cannot predict the unique H-bonding interactions between "N30" and KV1 channels.

The specificity of IbTX for BK versus KV channels is also defined by the acidic residues (D4, D6, and D24). Substitution of the ChTX residues (S4, N6, and S24) into IbTX causes a favorable change in binding free energy (ca. −4 kcal/mol) for KV1.3. In addition, the kinetics of binding of ChTX to *Shaker* KV1 show that the converse S24D mutation increased k_{off} >10-fold and destabilized the toxin−channel complex (*29*). Together, these data suggest that these ChTX residues form an important and unique part of the ChTX−KV1.3 interaction surface. Applying distance array analysis to the ChTX−KV1.3 complex (*22*), we found that no KV1.3 atoms were within van der Waals contact (3.5 Å) of the S4, N6, and S24 toxin atoms. The closest channel atoms were ≥6.5 Å from any ChTX atoms in S4, N6, and S24, suggesting that this model cannot account for these determinants of IbTX specificity.

In summary, the data in this study provide strong evidence to support the notion that four residues in IbTX (D4, D6, D24, and "G30") account for all of its specificity for BK versus KV1 channels. Moreover, they suggest that H-bonding interactions between N30 in the peptide and KV1 residues are unique and critical to the high-affinity block of these channels. Surprisingly, current structural models of α-KTx complexes do not accurately predict these IbTX specificity determinants. Because specificity determinants by definition

are unique, incorporation of these determinants in model building will lead to unique paradigms that afford a more accurate prediction of the structure of α-KTX−channel complexes.

ACKNOWLEDGMENT

We are grateful to Drs. Gregory Kaczorowski and Owen McManus (Ion Channels, Merck Research Laboratories) for their continued support and encouragement of this work. We thank Dr. Carol Deutsch (University of Pennsylvania, Philadelphia, PA), Dr. Toshinori Hoshi (University of Pennsylvania), and Dr. Christopher Lingle (Washington University, St. Louis, MO) for their valuable insights into and suggestions about the manuscript. J.P.F., B.T.P., W.S., and M.L.G. are employees of Merck & Co., Inc. and potentially own stocks and/or hold stock options in the company.

REFERENCES

1. Ashcroft, F. M. (2006) From molecule to malady, *Nature 440*, 440−447.
2. Brenner, R., Perez, G. J., Bonev, A. D., Eckman, D. M., Kosek, J. C., Wiler, S. W., Patterson, A. J., Nelson, M. T., and Aldrich, R. W. (2000) Vasoregulation by the β1 subunit of the calcium-activated potassium channel, *Nature 407*, 870−876.
3. Beeton, C., and Chandy, K. G. (2005) Potassium channels, memory T cells, and multiple sclerosis, *Neuroscientist 11*, 550−562.
4. Du, W., Bautista, J. F., Yang, H., Diez-Sampedro, A., You, S. A., Wang, L., Kotagal, P., Luders, H. O., Shi, J., Cui, J., et al. (2005) Calcium-sensitive potassium channelopathy in human epilepsy and paroxysmal movement disorder, *Nat. Genet. 37*, 733−738.
5. Huang, B., Qin, D., and El-Sherif, N. (2001) Spatial alterations of Kv channels expression and K^+ currents in post-MI remodeled rat heart, *Cardiovasc. Res. 52*, 246−254.
6. Garcia, M. L., and Kaczorowski, G. J. (2005) Potassium channels as targets for therapeutic intervention, *Sci. STKE 302*, 46.
7. Giangiacomo, K. M., Ceralde, Y., and Mullmann, T. J. (2004) Molecular basis of α-KTx specificity, *Toxicon 43*, 877−886.
8. Leonard, R. J., Garcia, M. L., Slaughter, R. S., and Reuben, J. P. (1992) Selective blockers of voltage-gated K^+ channels depolarize human T lymphocytes: Mechanism of the antiproliferative effect of charybdotoxin, *Proc. Natl. Acad. Sci. U.S.A. 89*, 10094−10098.
9. Raffaelli, G., Saviane, C., Mohajerani, M. H., Pedarzani, P., and Cherubini, E. (2004) BK potassium channels control transmitter release at CA3-CA3 synapses in the rat hippocampus, *J. Physiol. 557*, 147−157.
10. Schroeder, N., Mullmann, T. J., Schmalhofer, W. A., Gao, Y. D., Garcia, M. L., and Giangiacomo, K. M. (2002) Glycine 30 in iberiotoxin is a critical determinant of its specificity for maxi-K versus K(V) channels, *FEBS Lett. 527*, 298−302.
11. Garcia, M. L., Garcia-Calvo, M., Hidalgo, P., Lee, A., and MacKinnon, R. (1994) Purification and characterization of three inhibitors of voltage-dependent K^+ channels from *Leiurus quinquestriatus* var. *hebraeus* venom, *Biochemistry 33*, 6834−6839.
12. Park, C. S., Hausdorff, S. F., and Miller, C. (1991) Design, synthesis, and functional expression of a gene for charybdotoxin, a peptide blocker of K^+ channels, *Proc. Natl. Acad. Sci. U.S.A. 88*, 2046−2050.
13. Heinzel, S. S., Krysan, P. J., Calos, M. P., and DuBridge, R. B. (1988) Use of simian virus 40 replication to amplify Epstein-Barr virus shuttle vectors in human cells, *J. Virol. 62*, 3738−3746.
14. Hanner, M., Vianna-Jorge, R., Kamassah, A., Schmalhofer, W. A., Knaus, H. G., Kaczorowski, G. J., and Garcia, M. L. (1998) The β subunit of the high conductance calcium-activated potassium channel. Identification of residues involved in charybdotoxin binding, *J. Biol. Chem. 273*, 16289−16296.
15. Helms, L. M., Felix, J. P., Bugianesi, R. M., Garcia, M. L., Stevens, S., Leonard, R. J., Knaus, H. G., Koch, R., Wanner, S. G., Kaczorowski, G. J., et al. (1997) Margatoxin binds to a homomultimer of K(V)1.3 channels in Jurkat cells. Comparison with K(V)1.3 expressed in CHO cells, *Biochemistry 36*, 3737−3744.
16. Mullmann, T. J., Munujos, P., Garcia, M. L., and Giangiacomo, K. M. (1999) Electrostatic mutations in iberiotoxin as a unique tool for probing the electrostatic structure of the maxi-K channel outer vestibule, *Biochemistry 38*, 2395−2402.
17. Horovitz, A., and Levitzki, A. (1987) An accurate method for determination of receptor-ligand and enzyme-inhibitor dissociation constants from displacement curves, *Proc. Natl. Acad. Sci. U.S.A. 84*, 6654−6658.
18. Giangiacomo, K. M., Garcia, M. L., and McManus, O. B. (1992) Mechanism of iberiotoxin block of the large-conductance calcium-activated potassium channel from bovine aortic smooth muscle, *Biochemistry 31*, 6719−6727.
19. Giangiacomo, K. M., Fremont, V., Mullmann, T. J., Hanner, M., Cox, R. H., and Garcia, M. L. (2000) Interaction of charybdotoxin S10A with single maxi-K channels: Kinetics of blockade depend on the presence of the β1 subunit, *Biochemistry 39*, 6115−6122.
20. Kiss, L., Bennett, P. B., Uebele, V. N., Koblan, K. S., Kane, S. A., Neagle, B., and Schroeder, K. (2003) High Throughput Ion-Channel Pharmacology: Planar-Array-Based Voltage Clamp, *Assay Drug Dev. Technol. 1*, 127−135.
21. Eriksson, M. A., and Roux, B. (2002) Modeling the structure of agitoxin in complex with the Shaker K^+ channel: A computational approach based on experimental distance restraints extracted from thermodynamic mutant cycles, *Biophys. J. 83*, 2595−2609.
22. Yu, K., Fu, W., Liu, H., Luo, X., Chen, K. X., Ding, J., Shen, J., and Jiang, H. (2004) Computational simulations of interactions of scorpion toxins with the voltage-gated potassium ion channel, *Biophys. J. 86*, 3542−3555.
23. Nicholls, A., Sharp, K. A., and Honig, B. (1991) Protein folding and association: Isights from the interfacial and thermodynamic properties of hydrocarbons, *Proteins 11*, 281−296.
24. Aiyar, J., Withka, J. M., Rizzi, J. P., Singleton, D. H., Andrews, G. C., Lin, W., Boyd, J., Hanson, D. C., Simon, M., Dethlefs, B., et al. (1995) Topology of the pore-region of a K^+ channel revealed by the NMR-derived structures of scorpion toxins, *Neuron 15*, 1169−1181.
25. Ranganathan, R., Lewis, J. H., and MacKinnon, R. (1996) Spatial localization of the K^+ channel selectivity filter by mutant cycle-based structure analysis, *Neuron 16*, 131−139.
26. Hidalgo, P., and MacKinnon, R. (1995) Revealing the architecture of a K^+ channel pore through mutant cycles with a peptide inhibitor, *Science 268*, 307−310.
27. Wrisch, A., and Grissmer, S. (2000) Structural differences of bacterial and mammalian K^+ channels, *J. Biol. Chem. 275*, 39345−39353.
28. Lange, A., Giller, K., Hornig, S., Martin-Eauclaire, M. F., Pongs, O., Becker, S., and Baldus, M. (2006) Toxin-induced conformational changes in a potassium channel revealed by solid-state NMR, *Nature 440*, 959−962.
29. Goldstein, S. A., Pheasant, D. J., and Miller, C. (1994) The charybdotoxin receptor of a Shaker K^+ channel: Peptide and channel residues mediating molecular recognition, *Neuron 12*, 1377−1388.
30. Bontems, F., Roumestand, C., Gilquin, B., Menez, A., and Toma, F. (1991) Refined structure of charybdotoxin: Common motifs in scorpion toxins and insect defensins, *Science 254*, 1521−1523.
31. Johnson, B. A., and Sugg, E. E. (1992) Determination of the three-dimensional structure of iberiotoxin in solution by ^{1}H nuclear magnetic resonance spectroscopy, *Biochemistry 31*, 8151−8159.
32. Long, S. B., Campbell, E. B., and Mackinnon, R. (2005) Crystal structure of a mammalian voltage-dependent Shaker family K^+ channel, *Science 309*, 897−903.
33. Jiang, Y., Lee, A., Chen, J., Ruta, V., Cadene, M., Chait, B. T., and MacKinnon, R. (2003) X-ray structure of a voltage-dependent K^+ channel, *Nature 423*, 33−41.

BI700150T